In the work supported by the present OTKA grant the principle goals contained by the project proposal have been reached, regarding both understanding and overcoming the variability of UIC2-elicited Pgp inhibition. Moreover, a previously unforeseen efficiency of *in vivo* inhibition of Pgp activity, and markedly enhanced potency of tumor chemotherapy in xenotransplanted human tumors was observed. In addition, a general scheme has emerged concerning the trafficking routes of Pgp. The following main observations have been made:

I. Complete inhibition of P-glycoprotein by simultaneous treatment with a distinct class of modulators and the UIC2 monoclonal antibody *in vitro* and *in vivo*:

P-glycoprotein (Pgp) is one of the active efflux pumps that are able to extrude a large variety of chemotherapeutic drugs from the cells, causing multidrug resistance. The conformation sensitive UIC2 mAb potentially inhibits Pgp mediated substrate transport. However, this inhibition is usually partial and its extent is variable, since UIC2 binds only to 10-40 % of Pgps present in the cell membrane. The rest of Pgp molecules become recognized by this antibody only in the presence of certain substrates or modulators (including vinblastine, cyclosporine A (CsA) and SDZ PSC 833). Simultaneous application of any of these modulators and UIC2, followed by the removal of the modulator, results in a completely restored steady-state accumulation of various Pgp substrates (calcein-AM, daunorubicin and ^{99m}Tc-hexakis-2-methoxybutylisonitrille), indicating near 100% inhibition of pump activity (see Fig. 1.A and B). Remarkably, the inhibitory binding of the antibody is brought about by co-incubation with ~20 times lower concentrations of CsA or SDZ PSC 833 than what is necessary for Pgp inhibition when the modulators are applied

alone (see Fig. 1. right panels). The feasibility of such a combinative treatment for *in vivo* mdr reversal was substantiated by the dramatic increase of daunorubicin and doxorubicin accumulation in xenotransplanted Pgp^+ tumors in response to a combined treatment with UIC2 and CsA, both administered at doses ineffective when applied alone (see Fig. 2. upper panels).

In addition, the efficiency of this combined treatment was further tested *in vitro and in vivo*. The combined addition of UIC2 and low concentrations of SDZ PSC 833 or cyclosporine A significantly increased the cytotoxic effects of daunorubicin as compared to treatments with UIC2 or the modulator alone (see Fig. 2. lower left panel). Furthermore, in animals co-treated with doxorubicin and UIC2 + cyclosporin A the average weight of Pgp-expressing tumors was 5.4 ± 1.7 % of the drug untreated control, while doxorubicin treatment was almost ineffective as the tumor weight was 91.59 % ± 18.8 % of the drug untreated control (see Fig. 2. lower right panel). These observations establish the combined application of a class of modulators used at low concentrations and of the UIC2 antibody, as a novel, specific and effective way of blocking Pgp function *in vivo*. The results of the above study were summarized in a publication (Goda K et al. *J Pharmacol Exp Ther* 320: 81-88, (2007)), in a patent (patent number: 06740584 5-1222-US2006012738) and a new manuscript is in preparation (Tóth Á et al.: Overcoming Pgp-mediated drug resistance *in vivo* by the combined application of cyclosporine A and UIC2 monoclonal antibody).

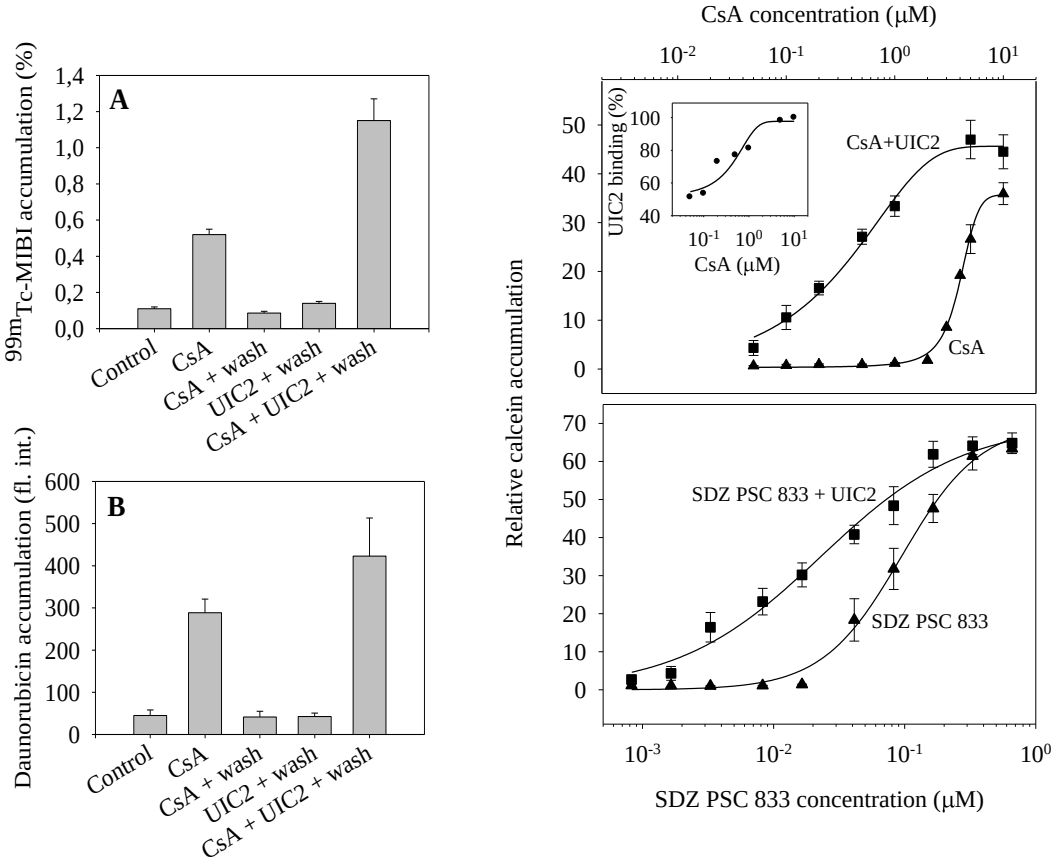

Fig. 1. The effect of cyclosporine A (CsA) and UIC2 on the accumulation of ^{99m}Tc-MIBI (***panel A***) and daunorubicin (***panel B***) into NIH 3T3 MDR1 cells**.** The effects of cyclosporine A (CsA**,** ***upper right panel***) and SDZ PSC 833 (***lower right panel***), added alone or in combination with UIC2 mAb, on calcein accumulation in NIH 3T3 MDR1 cells. The insert of ***upper right panel*** shows the UIC2 binding of cells (expressed as % of maximal labeling) visualized by indirect immunofluorescence in a parallel experiment.

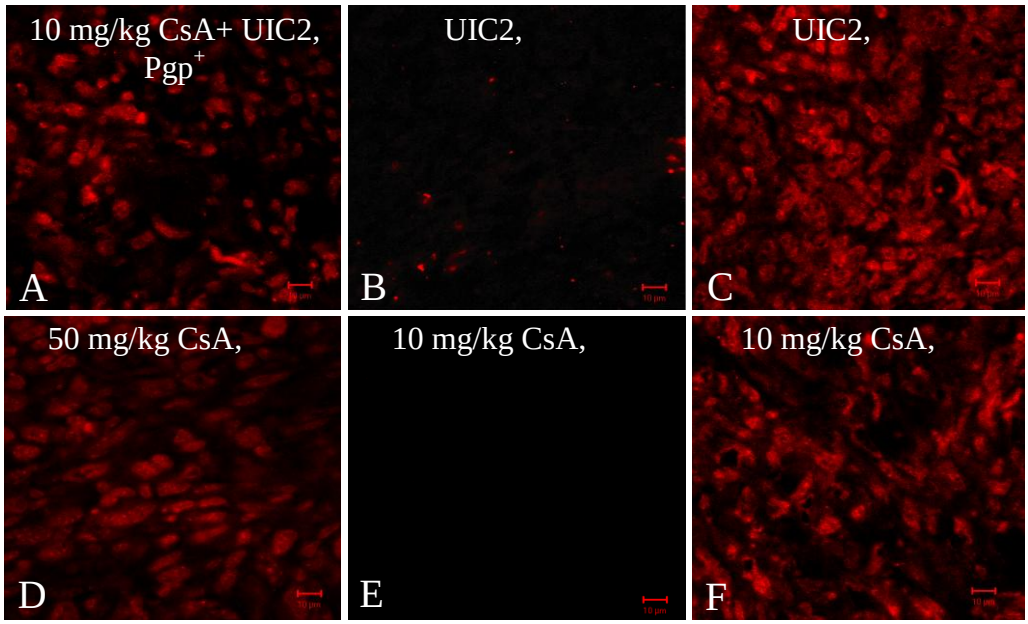

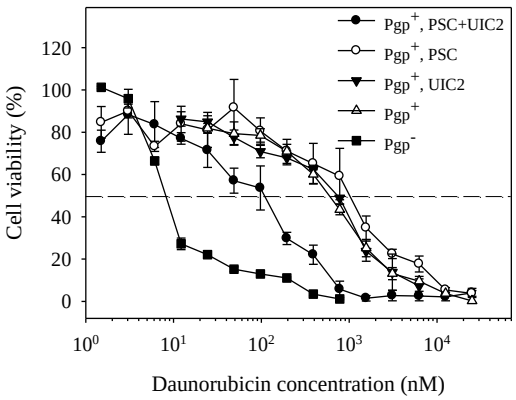

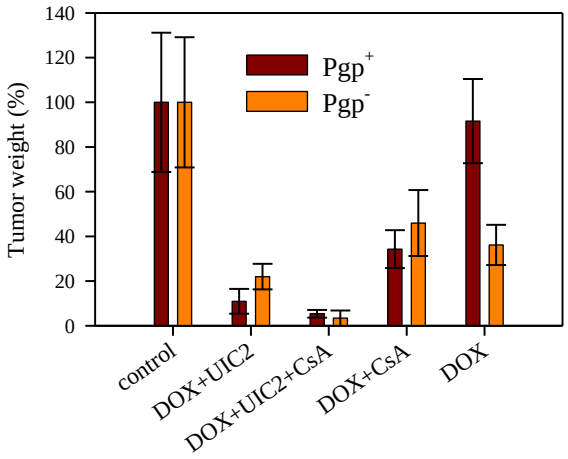

Fig.2. Confocal laser scanning microscopic images of daunorubicin accumulation in cryosections of NIH 3T3 MDR1 and NIH 3T3 tumors developed in SCID mice (***panels A, B, D, E*** and ***panels C, F,*** respectively). Tumors were palpable when mice were injected i.v. with various amounts of UIC2 antibody and/or CsA, followed by daunorubicin. Potentiation of cytotoxic effects of daunorubicin by combined treatment

with SDZ PSC 833 (15 nM) and UIC2 mAb (20 μg/ml) in MTT assay (***lower left panel***). Average tumor weight one week after treatment (expressed in %) compared to tumor weight measured in untreated SCID mice (***lower right panel***).

II. Elucidation of the conformational-topological heterogeneity of cell-surface P-glycoprotein molecules:

UIC2 (or its Fab fragment; unpublished observations) applied at saturation binds only to 10-40 % of Pgps present in the cell membrane (referred to herein as pool I Pgps). The entire population of the rest of Pgp molecules (called pool II) become recognized by this antibody in ATP-depleted cells and when cell labeling by UIC2 occurs in the presence of certain substrates or modulators mentioned in the previous section. In the absence of the above drugs, pool II Pgps may also be visualized by sequential labeling with UIC2 and any of a series of antibodies (e.g. MRK16, MM12.10 or 15D3) binding to partially overlapping binding sites. We have characterized the two Pgp populations distinguished by UIC2 binding in terms of membrane microdomain localization, cytoskeletal anchorage, intracellular molecular neighbours, trafficking characteristics and catalytic activity, in an attempt to understand the possible functional corollaries of this heterogeneity.

- Pgp molecules recognized by UIC2 in the absence of modulators (pool I) and those that bind this mAb in the presence of CsA-type drugs (pool II) occupy at least partly distinct territories within the cell membrane, according to our confocal microscopic, atomic force microscopy and homoFRET studies, membrane fractionation experiments and the results of the flow cytometric detergent elution (FCDR) experiments (see Fig.1,2 and Table 1).
- The heterogeneous membrane distribution of the two pools appears to preexist, rather than being induced by cross-linking of Pgps. The density gradient centrifugation data, as well as the differential anchorage characteristics revealed in the FCDR experiments (Fig. 2 and Table 1) corroborate the notion that the two Pgp pools belong to distinct membrane microenvironments. There is a preferential association of pool I Pgps with TX-100 resistant rafts and the cytoskeleton, as compared with pool II

molecules. This difference was reproduced using Fab fragments of the UIC2 antibody and also when Fab was used at 1/5 of saturation concentrations (Table 1), i.e. further decreasing the likelihood that aggregated Fabs might play a role, thus the valence of antibody binding doesn't appear to influence the anchorage features studied. Similar difference in the extent of anchorage between the two pools was found when pool II Pgps were detected using either UIC2 (in the presence of CsA) or the conformation-*in*sensitive MM12.10 or 15D3 antibody (see Table 1). The observed FCDR values are in agreement with the estimate of approximately 15% of all membrane protein being associated with the cytoskeleton via its distinct, membrane proximal elements, in a dynamic fashion.

- In TX-100 extraction experiments, upon modulation of the membrane cholesterol concentration by methyl-β-cyclodextrin, resistance of the two Pgp pools to detergent solubilization has become indistinguishable, suggesting that the different TX-100 resistance of the unperturbed pools is related to membrane features dependent on cholesterol content, implicating raft domains in the formation of pool I, in support of the density gradient centrifugation data (Fig. 2. C). In NP40 extraction experiments in contrast, the difference between the two pools is maintained in spite of the generally decreased detergent resistance upon reduction of membrane cholesterol levels (Fig. 2.D).
- It has been proposed that lipid rafts are composed of a highly ordered, Triton X-100-insoluble core region, rich in sphingolipids and cholesterol, which is surrounded by a less structured shell resistant to milder detergents (e.g. Brij 98), laterally merging with the bulk liquid disordered membrane phase. Our FCDR measurements suggest that most of the Pgps (>80 %) reside in the Brij 98 resistant rafts in both pools in agreement with previous studies carried out on different cell lines. Most pool I Pgp molecules reside in the TX-100 resistant core region of the rafts and pool II Pgps are either found in the less ordered shell area, or completely outside rafts, in the bulk lipid. This distribution may involve a dynamic equilibrium between the two Pgp pools suggested by the lack of sensitivity of the pool I/II ratio to brefeldin A treatment (Fig. 3. B). Since the amount of Triton-resistant molecules always exceeds

that of the NP40-resistant fraction, more Pgp molecules are anchored to the cytoskeleton via rafts than directly (compare Fig. 2. C and D).

- Pool I Pgps are obviously transport competent (see Fig. 3. B). The Pgp molecules making up pool II usually constitute the majority of all cell surface Pgps considering the typical >1.5 values of UIC2-shift, and are also transport competent (Fig. 3. B). However, pool II Pgps are in a state inaccessible to the antibody even upon prolonged incubation with the antibody both in the absence of substrates/modulators and in their constantly activated state (Fig. 3. B). At least a significant fraction of these pool II Pgp molecules efficiently executes transport of an indicator dye in view of the incomplete inhibition of pumping when UIC2 is applied in the absence of cyclosporin A.
- The ratio of Pgp in raft and non-raft domains appears to be tightly regulated in view of the constant pool I – pool II ratio across a wide range of Pgp expression (Fig. 4.), suggesting that heterogeneity is biologically important. The presence of Pgp in „raft" as well as in „non-raft" membrane microdomains with different cholesterol content may ultimately facilitate the recognition of substrates with diverse molecular structures, size and membrane partitioning characteristics. The topological heterogeneity described is likely to be related also to trafficking processes involving the pump molecule. This is suggested by the facts that pool I Pgps interact preferentially with cytoskeletal proteins (including vimentin and the actin binding proteins kaptin and filamin 1 (see Fig. 5 C and Table 2), in line with their higher NP-40 resistance (see Fig 2.D, and Table 1.) and enhanced internalization rate (see Fig. 5. A, B and D) . It seems likely that the rafts containing pool I Pgps serve as a platform for internalization.

III. New methods developed in connection with the current project:

The project has also lead to the development of several novel methods e.g. microbead based assays, indirectly linked to our studies on Pgp (Pataki et al. Cytometry A 68: 45-52, 2005; Székvölgyi et al. Cytometry A 69:1086-91, 2006). In membrane fractionation experiments the amount of certain membrane proteins was determined in the membrane fractions after they were captured on streptavidin conjugated microbeads. The

microbead-bound proteins (e.g. Pgp molecules) were detected by a fluorescently labeled secondary antibody and measured in a flow cytometer, avoiding the time-consuming Western blot experiments and densitometry.

Our work has lead to several important observations regarding the conformational-topological heterogeneity of cell surface Pgps, also pointing out novel perspectives for its inhibition *in vivo*. We identified several of its molecular neighbours and characterized the dynamics of its cell surface heterogeneity also in connection with the endo- and exocitotic processes involving the pump. These observations have lead to the suggestion of a novel paradigm, with ATP-nonbinding Pgp molecules preferentially subjected to endocytosis. The project has also lead to the development of several novel methods. The grant has been cited in several publications and also in manuscripts submitted or in preparation.

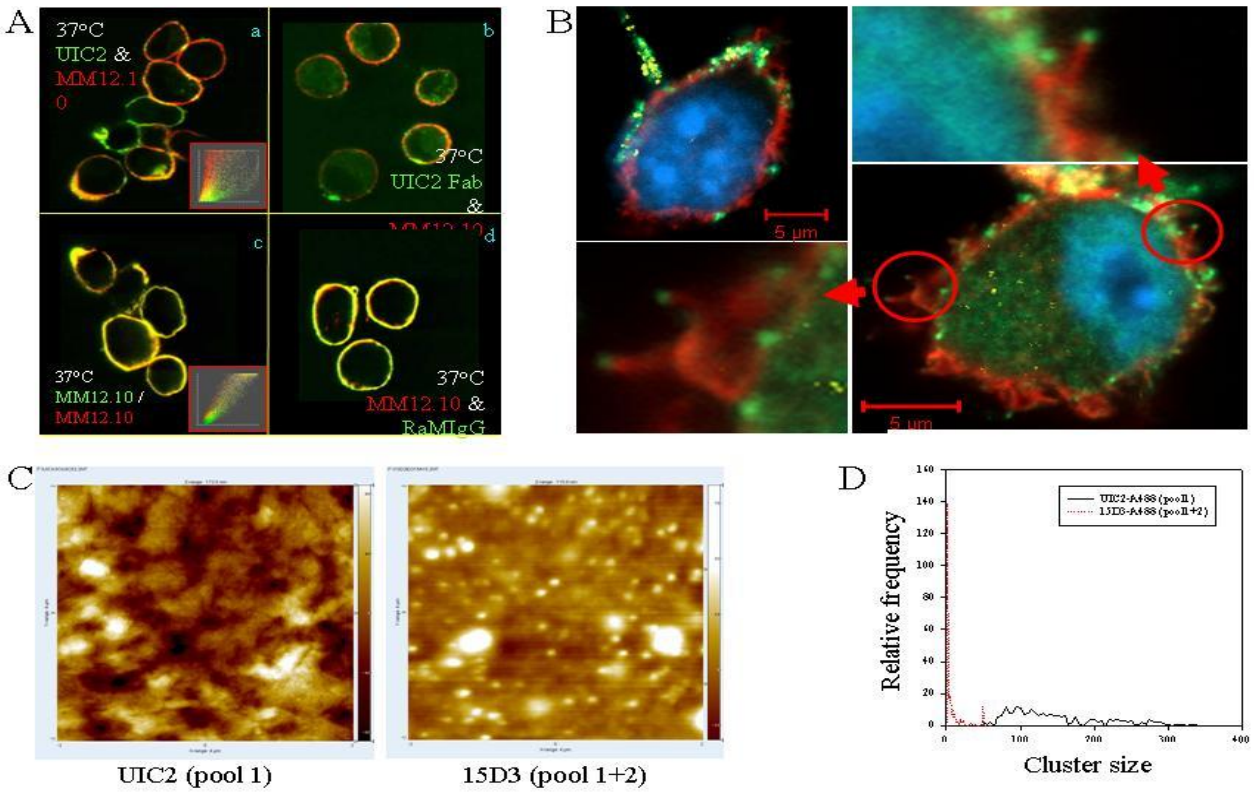

Fig. 1.

Fig, 1. Membrane distribution of Pgp molecules studied by confocal microscopy (***panels A and B***), atomic force microscopy (***C***) and flow cytometric homoFRET-anisotropy measurements (***D***). ***Panel A:*** Pool I Pgps were labeled with 5sFx-conjugated UIC2 mAb or its Fab fragment, while pool II Pgps were visualized by Cy5-conjugated MM12.10. The two pools appear to occupy partially different territories in the cell membrane (a and b pictures). In control experiments when cell surface Pgps were labelled with a 1:1 mixture of 5sFx- and Cy5-conjugated MM12.10 antibodies or Cy5-MM12.10 followed by FITC-RAMIgG, we experienced strong co-localization of the green and red signals (c and d pictures). The extent of separation was demonstrated in the correlation histograms of green and red intensities (see dot-plots in the inset, where each dot represents one pixel in the corresponding picture). ***Panel B:*** Pool I (green) and pool II (yellow) Pgp molecules appearing in separate patches are associated with the actin cytoskeleton (red). Nuclei were stained with Hoechst 33342 and F-actin was visualized by fluorescent dye-conjugated phalloidin. In the upper left image of panel B, patches of pool I and pool II Pgps are separated well from each other in a cell protrusion and in the cell surface. In lower right picture another cell is shown, where Pgps are clearly attached to the cortical actin cytoskeleton. ***Panel C:*** Cell surface distribution of UIC2 mAb labeled (pool I) and 15D3 mAb labeled (pool I+II) Pgps as measured by atomic force microscopy. The binding of primary antibodies was visualized by colloidal gold-conjugated secondary antibody (bead diameter was 30 ± 3 nm). ***Panel D***: Cluster size distribution of the two Pgp pools labeled by UIC2 (pool I) and 15D3 (pool I+II). Calculation was made based on

flow cytometric homoFRET-anisotropy measurements.

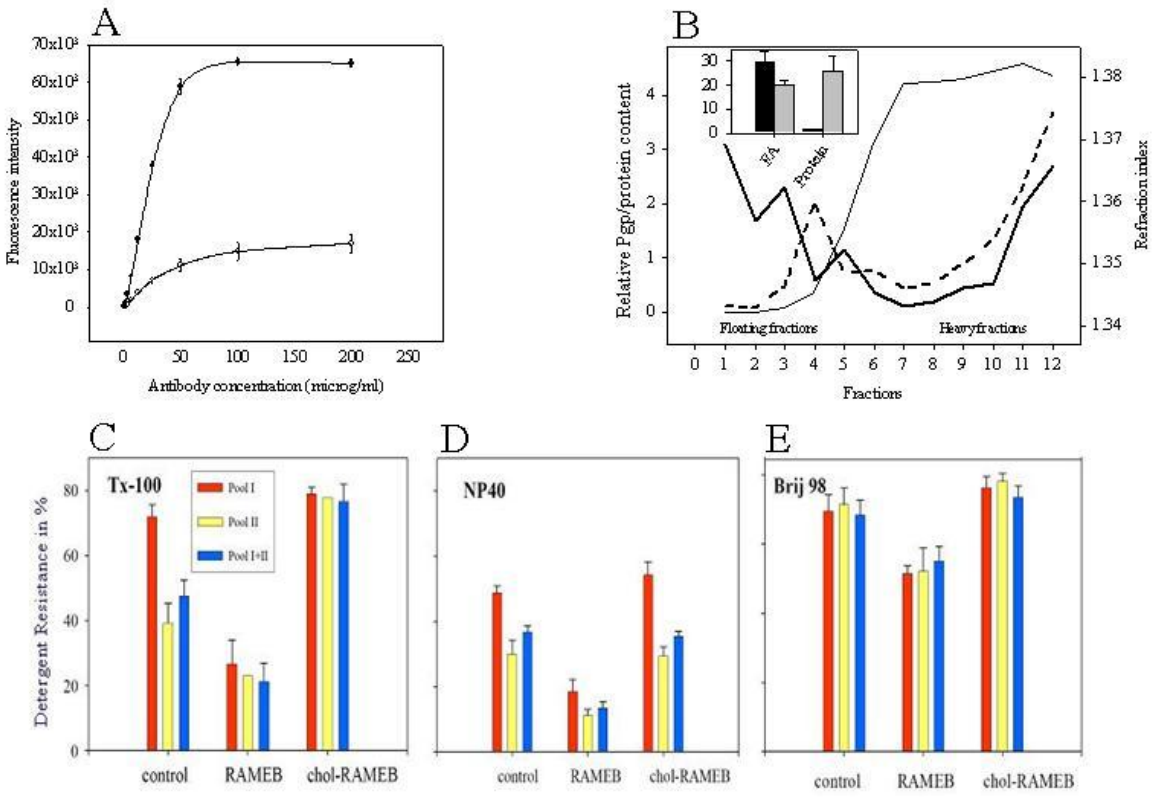

Fig. 2.

Fig. 2. Membrane microdomain distribution of pool I and pool II Pgps as determined in sucrose density gradient centrifugation experiments (***panel B***) and flow cytometric detergent resistance assay (***panel C-E***) in NIH 3T3 MDR1 cells. ***Panel B***: Pool I Pgps were labeled with biotinylated UIC2, while pool II Pgps were labeled with biotinylated 15D3 mAb (after covering pool I Pgps with UIC2 mAb). Cells were lysed in 1% Triton X-100 and membrane fractions were separated on discontinuous sucrose density gradient. The biotinylated primary antibodies were captured on streptavidin covered microbeads and their amount was determined applying A488-tagged secondary antibodies in a flow cytometer (Pool I: thick continous line; pool II Pgps: thick dashed line). Distribution of the sucrose density was tested measuring refraction index of the collected fractions. Higher refractive indicies show higher densities (thin continous line on the line graph, right scale). Pool I Pgps were preferentially observed in floating fractions (1-5) compared to heavy (6-12) fractions of the gradient. ***Insert of panel B***: Lipid and protein contents raft (black bars) and heavy fractions (grey bars). ***Panels C,D,E***: Effect of cholesterol modulation (depletion by RAMEB, saturation by chol-RAMEB) on the detergent resistance of the Pgp pools.

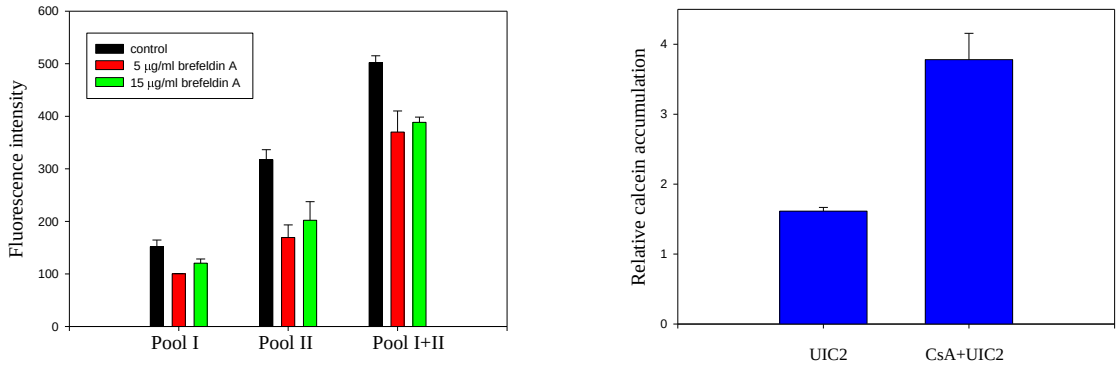

Fig. 3. ***left panel****:* The effect of 18 h brefeldin A treatment on the cell surface expression of Pgp pools. ***Right panel***: Effect of UIC2 binding on the calcein accumulation of PLB MDR1 cells. Cells were pre-labeled with UIC2 in the presence or absence of 5 μM CsA for 30 min and further incubated with calcein-AM for 20 min at 37 ˚C. Calcein accumulation was expressed relative to the antibody untreated control.

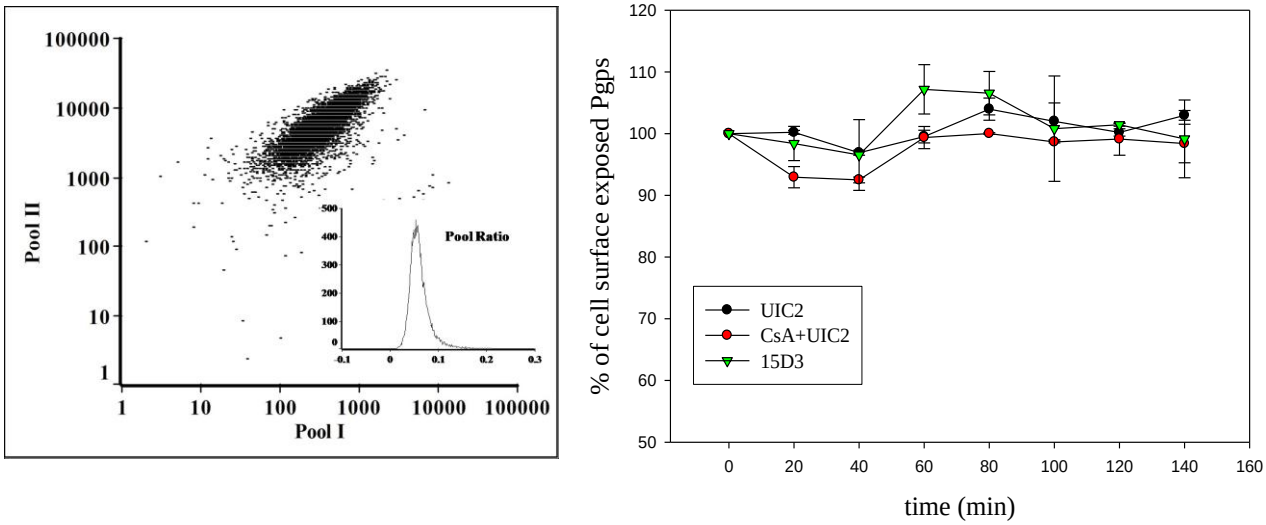

Fig 4. ***Left panel***: Ratio of the two Pgp pools labeled sequentially in NIH 3T3 MDR1 cells. Pool I Pgps were labeled with A488 conjugated UIC2 Fab, while pool II Pgps were labeled with A647 conjugated UIC2 Fab in the presence of 10 μM CsA. ***Right panel***: Cell surface expression level of pool I and pool I+II Pgps during prolonged incubations with the primary antibody at 37 ˚C. Samples were withdrawn at every 20 min washed and labeled with GamIg-A488 on ice. Fluorescence intensity of each sample was normalized to the first sample taken after 30 min incubation with the primary antibody.

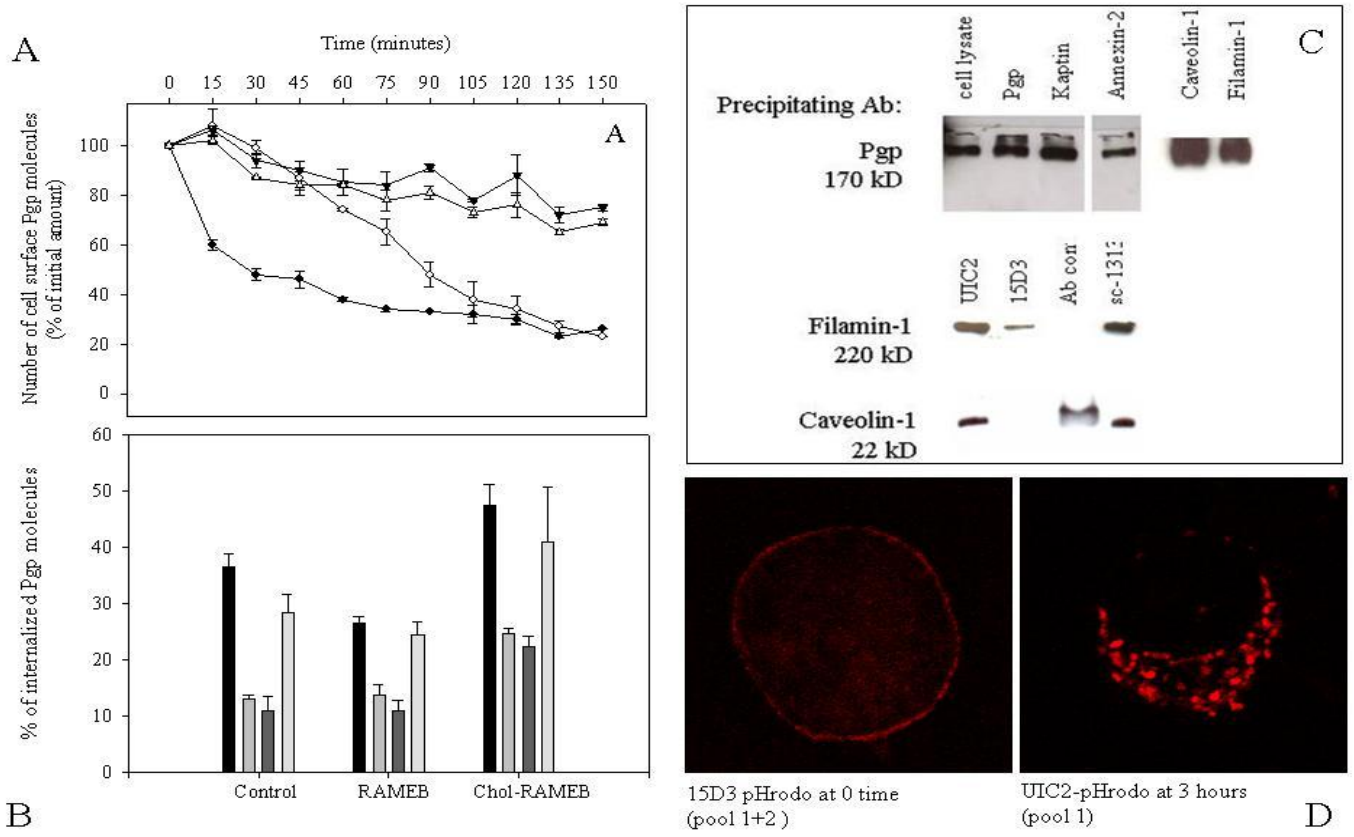

Fig. 5. The kinetics of endocytosis of the two cell surface Pgp pools was compared by measuring the loss of primary antibody labeled Pgps from the cell surface using fluorescent dye conjugated secondary antibody (***panel A***), by directly measuring the fraction of internalized Pgps after removal of antibodies exposed on the cell surface by acidic washes (***panel B***) and also following internalization Pgps by pH sensitive dye (pH-rodo) conjugated antibody (***panel D***). ***Panel C***: Western blot analysis of representative co-immunoprecipitation experiments. Caveolin1, filamin1, kaptin and annexin II was immunoprecipitated from TX-100 cell lysates. Immunoprecipitates were dissolved in Laemmli's sample buffer and run on 8% SDS/PAGE (upper panel). Pool I Pgps were immunoprecipitated by UIC2, while pool I+II Pgps by 15D3 or sc-13131 mAbs. Immunprecipitates were analyzed on 8% or 14 % SDS/PAGE when filamin 1 and caveolin1 was detected, respectively. Separated proteins were transferred to a nitrocellulose membrane and analyzed by western immunoblot (IB) analysis and enhanced chemiluminescence.

		Pool I	Pool II	Pool I+II
TX-100	UIC2 Fab (sat. cc)	58.1± 3.6	27.6±4.4	37.0±5.3
	UIC2 Fab (1/5 sat. cc)	66.6±16.5	24.7±8.3	37.3±5.7
	Whole Ab: UIC2	63.8± 1.4	36.3±4.6	37.1±2.0
	15D3	-	31.9	34.7±2.2
	MM12.10	-	22.8±1.8	31.3±1.3
	Cross-link (GamIg)	94.4±0.3	84.1±3.4	82.2±9.2
NP-40	UIC2 Fab (sat. cc)	34.4±7.3	12.0±4.89	15.9±3.4
	UIC2 Fab (1/5 sat. cc)	30.7±7.1	10.8±4.3	21.7±6.4
	Whole Ab: UIC2	45.7±4.3	27.4	27.3±1.9
	15D3	-	15.6	19.3±1.0
	MM12.10	-	12.70±1.9	24.0±4.3
	Cross-link (GamIg)	78.1±5.4	86.5±8.8	90.6±8.4

Table 1. Detergent resistance of the different Pgp pools. The fraction of mAb or Fab labeled molecules staying cell-bound after 30 min of TX-100 or NP40 treatment are shown in % of the initial fluorescence intensity. Pool I and pool II are Pgp molecules recognized by UIC2 in the absence of Pgp substrates or in the presence of CsA, respectively, while pool I+II designates all cell surface Pgps labeled with UIC2 in the presence of CsA or with other anti-Pgp antibodies (15D3 or MM12.10). In control experiments the UIC2 mAb labeled Pgps were cross-linked by GamIg. Means ± SEM are shown from 3-5 independent experiments, while data without SEM are the means of 2 independent experiments.

IP Sample	# of Peptides	Score	MW	pI	species	Acc. #	Protein name
UIC-2 1	13	204.81	48100.6	4.99	MOUSE	Q922R8	Protein disulfide-isomerase A6 precursor (Thioredoxin domain-containing protein 7)
UIC-2 2	4	50.44	53556.7	5.06	MOUSE	P20152	***Vimentin***
UIC-2 2	2	18.97	47545	4.86	MOUSE	Q8VCX6	***Kaptin***
UIC-2 3	30	408.75	53408.9	4.99	MOUSE	Q02819	Nucleobindin-1 precursor
UIC-2 3	2	29.96	51534.2	4.9	MOUSE	O88597	Beclin-1 (Coiled-coil myosin-like BCL2-interacting protein)
UIC-2 4	23	339.42	57143.9	4.8	MOUSE	P09103	Protein disulfide-isomerase precursor (PDI) (Prolyl 4-hydroxylase subunit beta) (Cellular thyroid hormone-binding protein) (p55) (Erp59)
15D3 1	2	22.34	28090.6	9	MOUSE	Q9D172	ES1 protein homolog, mitochondrial precursor
15D3 4	2	30.44	49563.7	6.26	MOUSE	Q8C1B7	Septin-11
15D3 5	16	249.48	46589.9	8.9	MOUSE	P19324	Serpin H1 precursor (Collagen-binding protein) (Colligin) (47 kDa heat shock protein) (Serine protease inhibitor J6)
15D3 9	6	86.12	38545.2	7.53	MOUSE	P07356	***Annexin A2*** *(Annexin II) (Lipocortin II) (Calpactin I heavy chain) (Chromobindin-8) (p36) (Protein I) (Placental anticoagulant protein IV) (PAP-IV)*
15D3 9	4	50.74	41870.3	8.8	MOUSE	Q91VA6	Polymerase delta-interacting protein 2

Table 2. Proteins interecting with pool I (UIC2) and pool II (15D3) Pgps expressed in NIH 3T3 mouse fibroblast cell line. UIC2 and 15D3 immunoprecipitates were separated by 2D gel electrophoresis. Protein spots unique for one of the immunprecipitates were excised and subjected to tryptic digestion and mass spectroscopic analysis. Mostly intracellular proteins were identified since membrane proteins hardly enter the 2D gels.